AD-A073 491 PENNSYLVANIA STATE UNIV UNIVERSITY PARK APPLIED RESE--ETC F/G 20/4
RADIATED NOISE DUE TO BOUNDARY-LAYER TRANSITION.(U)
JUL 79 G C LAUCHLE N00024-79-C-6043

UNCLASSIFIED ARL/PSU/TM-79-135 NL

| OF |
AD
A073491

END
DATE
FILMED
10-79
DDC

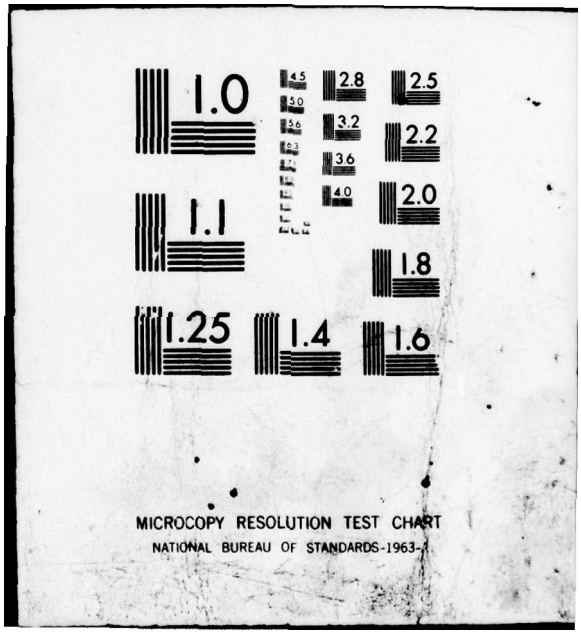
1.0
1.1
1.25
1.4
1.6
1.8
2.0
2.2
2.5
2.8
3.2
3.6
4.0
4.5
5.0
5.6
6.3
MICROCOPY RESOLUTION TEST CHART
NATIONAL BUREAU OF STANDARDS-1963-A

(12) B.S. LEVEL II

AD A073491

RADIATED NOISE DUE TO BOUNDARY-LAYER TRANSITION

G. C. Lauchle

Technical Memorandum
File No. TM 79-135
23 July 1979
Contract No. N00024-79-C-6043

Copy No. 49

DDC FILE COPY

The Pennsylvania State University
APPLIED RESEARCH LABORATORY
Post Office Box 30
State College, PA 16801

Approved for Public Release
Distribution Unlimited

NAVY DEPARTMENT

NAVAL SEA SYSTEMS COMMAND

UNCLASSIFIED

SECURITY CLASSIFICATION OF THIS PAGE (When Data Entered)

REPORT DOCUMENTATION PAGE

READ INSTRUCTIONS BEFORE COMPLETING FORM

1. REPORT NUMBER: TM 79-135
2. GOVT ACCESSION NO.:
3. RECIPIENT'S CATALOG NUMBER:
4. TITLE (and Subtitle): RADIATED NOISE DUE TO BOUNDARY-LAYER TRANSITION
5. TYPE OF REPORT & PERIOD COVERED: Technical Memorandum
6. PERFORMING ORG. REPORT NUMBER:
7. AUTHOR(s): G. C. Lauchle
8. CONTRACT OR GRANT NUMBER(s): N00024-79-C-6043
9. PERFORMING ORGANIZATION NAME AND ADDRESS:
Applied Research Laboratory
P. O. Box 30
State College, PA 16801
10. PROGRAM ELEMENT, PROJECT, TASK AREA & WORK UNIT NUMBERS:
11. CONTROLLING OFFICE NAME AND ADDRESS:
Naval Sea Systems Command
Washington, DC 20362
Code 63R-31
12. REPORT DATE: 23 July 1979
13. NUMBER OF PAGES: 45
14. MONITORING AGENCY NAME & ADDRESS (if different from Controlling Office): ARL/PSU/TM-79-135
15. SECURITY CLASS. (of this report): UNCLASSIFIED
15a. DECLASSIFICATION/DOWNGRADING SCHEDULE:

16. DISTRIBUTION STATEMENT (of this Report)

Approved for Public Release. Distribution Unlimited
Per NAVSEA - Aug. 29, 1979.

17. DISTRIBUTION STATEMENT (of the abstract entered in Block 20, if different from Report)

18. SUPPLEMENTARY NOTES

19. KEY WORDS (Continue on reverse side if necessary and identify by block number)

radiated noise
boundary layer
transition

20. ABSTRACT (Continue on reverse side if necessary and identify by block number)

A theory is presented for the noise radiated by incompressible boundary-layer transition that occurs on an infinite, rigid flat plate. It is hypothesized that it is the intermittency of the boundary-layer flow within the transition zone that is dominant in noise production. Using Lighthill's analogy, it is shown that dipole, quadrupole, and octupole sources are generated. The dipole sources are attributable to the shear stress fluctuations that occur in transitional flow while the others are due to fluctuating Reynolds stresses over (cont.)

DD FORM 1 JAN 73 1473 EDITION OF 1 NOV 65 IS OBSOLETE

391 007

UNCLASSIFIED

SECURITY CLASSIFICATION OF THIS PAGE (When Data Entered)

and their images. Under the assumption that dipole sources are more efficient than quadrupoles or octupoles when the Mach number is very small, the power spectrum of the radiated noise due to the dipole contribution is derived. The spectral level rises at 6 db/octave, peaks at a frequency corresponding to the time it takes for a turbulence burst to move through the transition region, and then drops off again at 6 dB/octave. The radiation efficiency is analyzed and found to be quite low; it is only 20 percent of that for a fully-developed turbulent boundary layer flow.

Subject: Radiated Noise Due to Boundary-Layer Transition

References: See page 32.

Abstract: A theory is presented for the noise radiated by incompressible boundary-layer transition that occurs on an infinite, rigid flat plate. It is hypothesized that it is the intermittency of the boundary-layer flow within the transition zone that is dominant in noise production. Using Lighthill's analogy, it is shown that dipole, quadrupole, and octupole sources are generated. The dipole sources are attributable to the shear stress fluctuations that occur in transitional flow while the others are due to fluctuating Reynolds stresses and their images. Under the assumption that dipole sources are more efficient than quadrupoles or octupoles when the Mach number is very small, the power spectrum of the radiated noise due to the dipole contribution is derived. The spectral level rises at 6 dB/octave, peaks at a frequency corresponding to the time it takes for a turbulence burst to move through the transition region, and then drops off again at 6 dB/octave. The radiation efficiency is analyzed and found to be quite low; it is only 20 percent of that for a fully-developed turbulent boundary layer flow.

Acknowledgement: The development of the analysis presented in this paper has been greatly influenced by discussions with many colleagues. Particular appreciation is expressed to Drs. D. G. Crighton, J. L. Lumley, W. K. Blake, and D. E. Thompson. The support of the U.S. Naval Sea Systems Command, Code 63R-31 is also gratefully acknowledged. The analysis, results, and conclusions presented in this memorandum are expanded and revised from those presented in two earlier ARL Technical Memoranda: ARL TM 79-204, 28 July 1978 and ARL TM 78-285, 7 November 1978.

TABLE OF CONTENTS

LIST OF FIGURES

I. INTRODUCTION

By contrast with the number of papers devoted to the investigation of noise radiated by a region of fully-developed turbulence, only a few have addressed the sound field generated by the laminar-to-turbulent transition zone [1 - 4]. Ffowcs Williams [1] discusses the transition zone noise in terms of the initial formation of turbulence spots. The elegant analysis of a three-dimensional disturbance growing in accordance with the equations of linear stability theory by Brooke Benjamin [5] was incorporated into Lighthill's theory [6] for the radiating component of flow noise. A quadrupole source was assumed and it was thus shown that sound radiation would occur essentially only when the wall was of pressure release type. For an assumed rigid surface the imaging effect transforms the quadrupoles into much less efficient octupole radiators. Furthermore, even for the soft surface, the analysis shows that it is only at the very beginning of spot formation where sound is generated. Farther downstream the spot grows exponentially, but the sound pressure is found to decrease exponentially with time. Of course it could be argued that the linear stability model breaks down as a spot develops which may account for this conclusion. Ffowcs Williams points out that the theory may be applicable only if sound is truly generated in the early stages of instability, but late enough such that the asymptotic theory of Brooke Benjamin is established, while at the same time the spot amplitude is still small.

Dolgova [4] considered the planar flow over a rigid surface and analyzed the sound radiated by only the Tollmien - Schlichting wave growth. As in linear stability models she let a pressure wave grow exponentially in the direction of flow, and then applied Fourier and Hankel transforms to obtain an expression for the sound pressure and directivity function. At low frequencies the pattern is

dipole while at higher frequencies the main lobe tilts to the downstream direction, gets sharper, and develops several side lobes. The resulting expression for the sound pressure, however, shows no Mach number dependence.

Natural transition is characterized by essentially three distinct, flow regimes. In the early stages of instability, the laminar boundary layer becomes disturbed in a linear, wavelike manner. It is here where the theory of Dolgova [4] is applicable. Farther downstream, these linear disturbances become more non-linear and three dimensional. The analysis of Ref. [1] appears to be applicable in this regime, but breaks down rapidly as turbulent bursts begin to form. Within the third flow regime, where the boundary layer intermittently alternates between laminar and turbulent, is where no fundamental flow noise theory has yet been developed. We hypothesize that this region of intermittent boundary-layer flow may give rise to sound radiation [2, 3]. We know from elementary boundary-layer theory that the mean velocity gradients and profiles are quite different between laminar and turbulent flow over surfaces. In intermittent flow, we would expect that the wall shear stress and the mean boundary layer velocities, both parallel and normal to the surface, undergo gross fluctuations in time. According to Lighthill's analogy [6], fluctuating velocities give rise to quadrupole noise sources, while fluctuating wall shear stresses give rise to dipole sources [7]. At very low Mach numbers, M, this latter source would be expected to dominate the noise field. This is deduced from the fact that the acoustic efficiency of dipole sources is of the order M^3, while that of quadrupole sources is of order M^5, viz., Ross [8].

In this paper we will approach analytically the problem of noise generated by intermittent boundary-layer flow as it occurs in natural transition on a flat plate.

We will assume the plate to be infinite in extent and to be acoustically rigid. We will further assume that incompressible hydrodynamics will describe the transitional process. Our goal is to derive expressions for the radiated noise spectrum and acoustic efficiency. The spectrum, because of our infinite extent assumption, will be derived in terms of the sound pressure radiated per unit spanwise width of transition. A comparison of predicted spectra with experimental data obtained on the surface of a buoyantly-propelled vehicle is also presented.

II. ANALYSIS

Consider the uniform flow over a flat plate. If a laminar boundary layer begins to form at the origin of our Cartesian coordinate system, and if the flow direction is in the x_1-direction, then the flow will ultimately become nonlinearly unstable at the downstream line $x_1=x_0$ (see Fig. 1). There is then a short distance, Δx, over which turbulent "bursts" occur. Along $x_1 = x_0 + \Delta x$, the flow becomes fully turbulent while for $x_1 < x_0$, the flow is assumed completely laminar. In the analysis to follow, we will treat $\delta \Delta x dx_3$ as our source volume, where δ is the boundary layer thickness.

The equation that describes the sound radiation from fluid-dynamic sources is the well-known Lighthill equation [6]:

$$\frac{\partial^2 \rho'}{\partial t^2} - c^2 \frac{\partial^2 \rho'}{\partial x_i^2} = \frac{\partial^2 T_{ij}}{\partial x_i \partial x_j} \quad , \tag{1}$$

where ρ' is the fluctuating density, t is time, c is the sound velocity in the medium surrounding the source region, and T_{ij} is Lighthill's stress tensor given by:

$$T_{ij} = \rho u_i u_j - \sigma_{ij} + (p' - \rho' c^2)\delta_{ij} \quad , \tag{2}$$

where ρ is the mean density.

Composing this tensor is $\rho u_i u_j$, the fluctuating Reynolds stress tensor; σ_{ij}, the fluctuating viscous shear stress tensor; and $(p' - \rho' c^2)$, a term that relates to heat conduction or nonlinearity. For hydrodynamic flows, this last term is zero which means that the fluctuating density is related to the fluctuating pressure by

$$p' = \rho' c^2 \quad . \tag{3}$$

From this point on, we will drop the prime from the fluctuating quantities, and solve Eq. (1) for the acoustic pressure through use of Eq. (3).

A. T_{ij} for Boundary-Layer Transition

Within the region $x_0 \leq x_1 \leq x_0 + \Delta x$, the flow intermittently changes from laminar to turbulent regimes. A typical turbulence burst is shown schematically in Fig. 2. A burst will grow as it travels downstream at a mean convection velocity, u_c. The locus of a typical burst forms a wedge of apex angle 2α. Emmons [9] first observed α to be on the order of 9.6° for flat plate flows. This was reconfirmed later by Schubauer and Klebanoff [10], although it should be pointed out that Farabee, et.al. [11] found propagation angles significantly greater than this.

In reference to the elevation view of Fig. 2, we might anticipate that at a given point on the x_1-axis, the mean velocity profile and the wall shear stress will undergo gross fluctuations in time as bursts are swept by. We will assume that these fluctuations are much larger than the velocity and shear stress fluctuations that occur within a burst itself or within the fully-developed turbulent boundary layer that occurs at $x_1 > x_0 + \Delta x$. For example, the wall shear stress under a turbulent boundary layer can be calculated from [12]:

$$\tau_T(x_1) = 0.0288\rho u_0^2 (u_0 x_1/\nu)^{-1/5} , \tag{4}$$

while at some other instant of time, when the boundary layer is laminar at x_1:

$$\tau_L(x_1) = 0.332\rho\nu u_0 (\nu x_1/u_0)^{-1/2} , \tag{5}$$

where ν is the kinematic viscosity. Thus, as the flow regime alternates between laminar and turbulent, we might expect fluctuations in the wall shear stress on the order of $\sigma(x_1)$, where

$$\frac{\sigma(x_1)}{\tau_T(x_1)} \equiv \frac{\tau_T - \tau_L}{\tau_T} = 1 - 11.53(Re_{x_1})^{-3/10} , \tag{6}$$

and $Re_{x_1} = u_0 x_1/\nu$ which is the local value of length Reynolds number. Typically, $Re_{x_0} \simeq 3 \times 10^6$, so $\sigma(x_0) \simeq 0.9\tau_T(x_0)$. Although not quantitatively proven, we would expect that fluctuations of this magnitude far exceed the wall shear stress fluctuations that may occur beneath a fully-developed turbulent boundary layer (compare, for example, Fig. 16.17 with Fig. 18.4 of Schlichting [12]).

Consequently, Eq. (2) for T_{ij} may be written

$$T_{ij} = \rho u_i u_j - \tau_0(x_i,t) , \tag{7}$$

where

$$\tau_0(x_i,t) = \sigma_{12}|_{x_2 = 0} >> \sigma_{ij}(ij\neq 12) \tag{8}$$

which is the fluctuating wall shear stress due to the creation and convection of turbulence bursts. If we further assume (because of the slow rate at which a burst spreads laterally) that the mean velocity fluctuation in the x_3-direction is small compared to u_1 and u_2, then T_{ij} will have only three dominant components in addition to $\tau_0(x_1,t)$.

We have not yet been explicit regarding the time dependence of τ_0, u_1, and u_2. It will prove expedient first to solve Eq. (1) subject to our assumed form of T_{ij} and the appropriate acoustic boundary conditions.

B. Formal Solution

The solution of Eq. (1) for flow over arbitrary surfaces was first constructed by Curle [13]. Powell [14] showed that when the surface is rigid and planar, one could consider a new extended flow field obtained by reflection of the original one in the plane $x_2 = 0$, as illustrated in Fig. 3(a). Using Powell's result, we find

$$p(r,t) = c^2\rho'(r,t) = \frac{\rho}{4\pi}\frac{\partial^2}{\partial x_i \partial x_j}\iiint_{V+V'}\frac{u_i u_j}{r}\,dV - \frac{1}{2\pi}\frac{\partial}{\partial x_1}\iint_S \frac{\tau_0}{r}\,dS, \qquad (9)$$

where the integrands are functions of the retarded time variable (t-r/c) and primes refer to the image-flow side of the plane. The radial coordinate defining the point of observation is $r = |\bar{x} - \bar{\eta}|$, where $\bar{\eta}$ denote the source volume coordinates. By making the far-field assumption, we can let $r \simeq r' \simeq |\bar{x}|$, and then by making the standard transformations from spatial derivatives to time derivatives, Eq. (9) becomes:

$$4\pi rc^2 p(r,t)/\rho = \left(\frac{x_1}{r}\right)^2 \frac{\partial^2}{\partial t^2} \iiint_V u_1^2 dV + 2\frac{x_1 x_2}{r^2} \frac{\partial^2}{\partial t^2} \iiint_V u_1 u_2 dV$$

$$+ \left(\frac{x_2}{r}\right)^2 \frac{\partial^2}{\partial t^2} \iiint_V u_2^2 dV + \left(\frac{x_1}{r}\right)^2 \frac{\partial^2}{\partial t^2} \iiint_{V'} (u_1')^2 dV' + 2\frac{x_1 x_2}{r^2} \frac{\partial^2}{\partial t^2} \iiint_{V'} u_1' u_2' dV'$$

$$+ \left(\frac{x_2}{r}\right)^2 \frac{\partial^2}{\partial t^2} \iiint_{V'} (u_2')^2 dV' + 2\frac{c}{\rho} \left(\frac{x_1}{r}\right) \frac{\partial}{\partial t} \iint_S \tau_0 dS \quad . \qquad (10)$$

Each of the terms composing Eq. (10) represent a hydrodynamically - generated acoustic source. The direction cosine preceeding each integral tells us the order and orientation of each of these sources. We see that the first and fourth terms have a $\cos^2\theta$ directivity characteristic (see Fig. 1 for definition of θ), indicating that they are longitudinal quadrupoles with axes parallel to the surface. These two sources, one being in the image flow combine constructively to form a single longitudinal quadrupole of twice the strength of one alone. The second and fifth terms represent lateral quadrupoles because of the cross-term products and directivity function $\sin\theta \cos\theta$. However, when combining a lateral quadrupole with its image, a less efficient octupole results. We can safely neglect those source terms involving $u_1 u_2$ and $u_1' u_2'$ under our low Mach number assumption. The third and sixth terms also represent longitudinal quadrupoles, but because $(x_2/r)^2 = \sin^2\theta$ their axes are perpendicular to the surface; when combined, another inefficient octupole results [15]. The last term of Eq. (10) includes the image contribution and describes a dipole source with axis parallel to the surface. Fig. 3(b) illustrates in an elementary manner the combination of these various sources.

Our solution to Eq. (1) thus reduces to the sum of a volume integral describing longitudinal quadrupoles and a surface integral describing dipoles, i.e.,

$$p(r,t) = \frac{\rho\cos^2\theta}{2\pi rc^2}\frac{\partial^2}{\partial t^2}\iiint_V u_1^2(\eta_i, t-r/c)dV(\eta_i)$$

$$+ \frac{\cos\theta}{2\pi rc}\frac{\partial}{\partial t}\iint_S \tau_0(\eta_i, t-r/c)dS(\eta_i) \quad . \tag{11}$$

As pointed out in the INTRODUCTION, we can expect the dipole contribution of Eq. (11) to be of the order M^{-2} more efficient than the quadrupole contribution. As a first approximation, we would like to accept this supposition, and examine in detail

$$p(r,t) \simeq \frac{\cos\theta}{2\pi rc}\frac{\partial}{\partial t}\iint_S \tau_0(\eta_i, t-r/c)dS(\eta_i) \quad , \tag{12}$$

when $M << 1$.

C. Proposed Model for the Wall Shear Stress Fluctuations

We have developed the solution given by Eq. (12) upon the notion that it is the intermittency of the boundary layer within the transition zone that creates noise. Intermittent boundary-layer flow is a situation where we can construct a mathematical model for the fluctuating physical parameters of interest. This model is analogous to that which the experimentalist uses to distinguish time intervals when his sensor is in irrotational fluid from those when it is in turbulent fluid.

Clearly, this is a zero-one function which we shall call the indicator function, $I(x_i,t)$. The use of such a function to describe intermittently turbulent flows is not new, viz., Refs. [16-18], among others. However, as will become apparent below, we will require the space-time correlation functions of $I(x_i,t)$, and these functions have not been so well investigated for boundary-layer transition [19].

Typically, the indicator function at a given point, x_i, in the source volume may be illustrated as in Fig.4. This function is zero when the flow is laminar and is unity when turbulent. Also shown in this illustration is the first time derivative of $I(x_i,t)$ which is a random sequence of alternating Delta functions. Because Eq. (12) needs only to be evaluated on the surface, the functional dependence of I on x_2 is not required. It is reasonable to let I be statistically homogeneous in x_3 because of our infinite plane surface assumption; however, I must necessarily be non-homogeneous in x_1.

The non-homogeneity of I in the x_1-direction is due to the fact that the boundary layer ultimately changes from fully laminar to fully turbulent. As x_1 increases beyond x_0 more and more impulse functions fill in the time scale. The time-average value of $I(x_1,t)$ is appropriately called the intermittency factor, i.e.,

$$\gamma(x_1) = \lim_{T\to\infty} \frac{1}{T} \int_0^T I(x_1,t)dt = \lim_{T\to\infty} \frac{1}{T} \int_0^T I^2(x_1,t)dt \quad , \tag{13}$$

and represents the fraction of time that the flow is turbulent. This is a predictable function for boundary-layer transition on flat plates [9] as well as for axisymmetric bodies [20]. Another important mean property of $I(x_1,t)$ is the "burst frequency," $N(x_1)$. This function describes the expected number of bursts that

occur at a given point per unit time. It too, may be predicted for most hydrodynamic flows [9, 11, 20]. Fig. 5 shows, in principle, how the indicator function varies in time and space; also shown are typical distributions of γ and N.

With these definitions for $I(x_i,t)$, and its mean properties, we propose that

$$\tau_0(x_i,t) = [1-I(x_i,t)]\ \tau_L(x_i) + I(x_i,t)\ \tau_T(x_i) \tag{14}$$

where i may take on the values 1 and 3. By taking the time derivative of Eq. (12) inside the integrals, we find:

$$\frac{\partial \tau_0}{\partial t} = (\tau_T-\tau_L)\ \frac{\partial I}{\partial t} = \sigma(x_i)\ \dot{I}(x_i,t) \quad , \tag{15}$$

where σ was first defined in Eq. (6).

As this point it is important to emphasize that Eq. (14) implies that the wall shear stress is capable of changing from a laminar value to a turbulent value in an infinitesimally-short period of time ($\dot{I}$'s are Delta functions). Obviously, this would seem physically impossible. However, we do know, from oscillograph traces of the velocity and/or pressure fluctuations that occur in transition flows, that the flow state can change in extremely short periods of time as turbulent bursts are created at or swept by the measuring sensor [10-12]. Eq. (14), although idealistic, may be quite adequate for estimating the low-frequency portion of the radiated noise spectrum. The techniques developed by Schottky [21] in his classic analysis of shot noise would seem appropriate here.

As a final point regarding Eq. (14), we note that its time average is simply:

$$\langle\tau_0(x_1,t)\rangle = [1-\gamma(x_1)]\ \tau_L(x_1) + \gamma(x_1)\ \tau_T(x_1) \tag{16}$$

which is identical to that suggested by Emmons [9] for the transition region. Several experiments have verified this equation, e.g., Dhawan and Narasimha [22].

D. Power Spectral Density of the Radiated Noise

After the substitution of Eq. (15) into Eq. (12) we find that the radiated acoustic pressure is of the form:

$$p(r,t) = \frac{\cos\theta}{2\pi rc} \int_0^{\Delta x} \int_{-\infty}^{\infty} \dot{I}(\eta_1,\eta_3,t-r/c)\ \sigma(x_0+\eta_1)\ d\eta_1 d\eta_3 \quad , \tag{17}$$

where the origin of our coordinate system has been displaced x_0-units downstream in order to simplify the variables in our integrals. The one-sided physical spectrum can be calculated from the Fourier integral [23]:

$$G(r,f) = 2 \int_{-\infty}^{\infty} \langle p(r,t)\ p(r,t+\tau)\rangle\ e^{i\omega\tau}\ d\tau \quad , \tag{18}$$

where $\langle p(r,t)\ p(r,t+\tau)\rangle$ is the autocorrelation function of $p(r,t)$, f is the frequency, and $\omega = 2\pi f$. In general,

$$\langle gg'\rangle \equiv \langle g(t)\ g(t+\tau)\rangle = \lim_{T\to\infty} \frac{1}{T} \int_0^T g(t)\ g(t+\tau)dt \quad . \tag{19}$$

Therefore, for $p(r,t)$:

$$\langle pp' \rangle = \frac{\cos^2\theta}{4\pi^2 r^2 c^2} \int\int\int\int \langle \dot{I}(\eta_1,\eta_3,t-r/c)\ \dot{I}(\phi_1,\phi_3,t-r/c+\tau)\rangle$$

$$\cdot\sigma(x_0+\eta_1)\ \sigma(x_0+\phi_1)\ d\eta_1 d\eta_3\ d\phi_1 d\phi_3 \quad , \tag{20}$$

where for the time being, we will not show the limits of integration. It will prove useful to change the ϕ_i-variables to spatial-separation variables $\xi_i = \phi_i - \eta_i$, such that Eq. (20) becomes:

$$\langle pp' \rangle = \frac{\cos^2\theta}{4\pi^2 r^2 c^2} \int\int\int\int \langle \dot{I}(\eta_1,\eta_3,t-r/c)\ \dot{I}(\eta_1+\xi_1,\eta_3+\xi_3,t-r/c+\tau)\rangle$$

$$\cdot\sigma(x_0+\eta_1)\ \sigma(x_0+\eta_1+\xi_1) d\eta_1 d\eta_3\ d\xi_1 d\xi_3 \quad . \tag{21}$$

If we assume $\dot{I}(x_i,t)$ to be stationary in time and homogeneous in x_3, Eq. (21) may be written without any loss of generality as:

$$\langle pp' \rangle = \frac{\cos^2\theta}{4\pi^2 r^2 c^2} \int\int\int\int \langle \dot{I}(\eta_1,0,0)\ \dot{I}(\eta_1+\xi_1,\xi_3,\tau)\rangle$$

$$\cdot\sigma(x_0+\eta_1)\ \sigma(x_0+\eta_1+\xi_1)\ d\eta_1\ d\eta_3\ d\xi_1 d\xi_3 \quad . \tag{22}$$

(We note that it makes no difference, in a stationary process, when one begins analyzing an event, whether at t = t or at t' = t + r/c.). Because $\langle \ddot{I}\ddot{I}' \rangle = -\partial^2 \langle II' \rangle / \partial\tau^2$, the power spectrum of a process composed of Delta functions is equivalent to ω^2 times the power spectrum of the same process composed of unit impulse functions. Thus, Eq. (18) becomes

$$G(r,f) = \frac{\omega^2 \cos^2\theta}{2\pi^2 r^2 c^2} \int\int\int\int\int_{-\infty}^{\infty} \langle I(\eta_1,0,0)\ I(\eta_1+\xi_1,\xi_3,\tau)\rangle$$

$$\cdot\sigma(x_0+\eta_1)\ \sigma(x_0+\eta_1+\xi_1)\ e^{i\omega\tau}\ d\eta_1 d\eta_3\ d\xi_1 d\xi_3\ d\tau \quad . \tag{23}$$

It is now assumed that <II'> can be treated in much the same way as the analogous space-time correlation function that occurs in the case of a homogeneous, fully-developed turbulent boundary layer. In particular, we assume that <II'> can be separated [24, 25], i.e., let

$$\langle II'\rangle = R_1(\eta_1,\xi_1,\tau)\ R_2(\eta_1,\xi_3) \quad . \tag{24}$$

The lateral term, R_2, can be integrated in the form:

$$\int_{-\infty}^{\infty} R_3(\eta_1,\xi_3)\ d\xi_3 = \int_{-L_3}^{L_3} d\xi_3 = 2L_3(\eta_1) \quad , \tag{25a}$$

where L_3 is a transition-width integral scale. Chen and Thyson [20] discuss a spanwise length scale in the region of transition where the bursts begin to overlap; that is, where $\eta_1 \to \Delta x$. They write this scale in the form $\Lambda \simeq 1.5\ \Delta x \tan\alpha$. Let us set $L_3(\Delta x) = \Lambda$ and $L_3(0) = 0$. It would then seem that

$$L_3(\eta_1) \simeq 1.5\eta_1 \tan\alpha$$

$$\simeq \eta_1/4 \text{ for } \alpha = 9.6^\circ \quad . \tag{25b}$$

It can be shown, through a Taylor series expansion, that $\sigma = \tau_T - \tau_L$ is only weakly-dependent on its argument through the range of integration required in Eq. (23). In particular,

$$\sigma(x_0+\varepsilon) \simeq Ax_0^{-1/5}\left(1 - \frac{\varepsilon}{5x_0}\right) - Bx_0^{-1/2}\left(1 - \frac{\varepsilon}{2x_0}\right) \quad , \tag{26}$$

where

$$A = 0.0288\rho u_0^2 Re_u^{-1/5} \quad ,$$

$$B = 0.332\rho\nu u_0 Re_u^{1/2} \quad ,$$

with

$Re_u = u_0/\nu$, which is the unit Reynolds number.

The maximum value which ε assumes is Δx, the streamwise extent of the transition zone. For incompressible boundary-layer transition, Δx can be estimated from the following emperical relationship [20, 22] between the Reynolds number based on the transition point, x_0, and that based on Δx:

$$Re_{\Delta x} = 60 Re_{x_0}^{2/3} \quad . \tag{27}$$

This relation can be rewritten in the form

$$\frac{\Delta x}{x_0} = \frac{\varepsilon_{max}}{x_0} = 60 Re_{x_0}^{-1/3} \quad .$$

In connection with the discussion following Eq. (6), we would expect the first term (the turbulent wall shear stress) of Eq. (26) to dominate, so that

$$\sigma(x_0+\epsilon_{max}) \simeq Ax_0^{-1/5}\left(1-12Re_{x_0}^{-1/3}\right)$$

$$\simeq \sigma(x_0) \quad . \tag{28}$$

This approximation implies that if the boundary layer were completely laminar or completely turbulent over the distance Δx, then the mean value of the wall shear stress changes insignificantly over this streamwise distance. It is analogous to the parallel-flow assumption commonly used in analyses related to fully-developed turbulent boundary-layer flow.

Differentiating Eq. (23) with respect to x_3, and making use of Eq's. (25) and (28), yields:

$$\frac{\partial G(r,f)}{\partial x_3} \simeq \frac{\omega^2\cos^2\theta\sigma^2(x_0)}{4\pi^2 r^2 c^2}\int\int\int_{-\infty}^{\infty} \eta_1 R_1(\eta_1,\xi_1,\tau)\, e^{i\omega\tau}\, d\eta_1\, d\xi_1\, d\tau \quad , \tag{29}$$

which is the power spectral density of the sound radiated per unit spanwise width of boundary-layer transition.

1. Longitudinal Space-Time Correlation Function

The longitudinal space-time correlation function, $R_1(\eta_1,\xi_1,\tau)$, has not been previously investigated in enough detail for us to write down an explicit expression for it; however, Shivitz [26] presented a very limited set of data for R_1 at $\eta_1 = 0.6\Delta x$. Although somewhat heuristic we will attempt to formulate a model for R_1 based on our physical notions of the transition process. In regards to the

τ-dependence, we let the random sequence of impulse functions that make up our indicator function be Poisson distributed. We select this distribution because it is a discrete distribution (which it necessarily must be) for a number of events (turbulent bursts) that all happen at random times with an average of N events per unit time (our burst frequency). Indeed, the experimental investigation of turbulence bursts by DeMetz, et.al. [27] does suggest a Poisson process. Under this assumption, the classical correlation function for a random telegraph signal may be used (see Rice [28]), which is of the form $\exp(-2N|\tau|)$.

The non-homogeneity of R_1 in η_1 necessitates weighing it by the standard deviation:

$$\langle I^2(\eta_1,0)\rangle = \gamma(\eta_1) \quad , \tag{30}$$

which is the intermittency factor [from Eq. (13)]. At a given location, η_1, we expect that the correlation should peak when $\tau = \xi_1/u_c$ which represents the lag time for a given turbulence burst to convect over the distance ξ_1 at a convection speed u_c. However, in a frame of reference moving at the convection speed we would experience a so-called "moving-axis decorrelation [29]" which accounts for the fact that a burst cannot remain perfectly correlated as the distance ξ_1 increases beyond some characteristic scale. With these notions, Eq. (31) appears to satisfy what is required:

$$R_1(\eta_1,\xi_1,\tau) \simeq \gamma(\eta_1)\, e^{-\alpha^*|\xi_1|}\, e^{-2N|\tau-\xi_1/u_c|} \quad , \tag{31}$$

where α^* and N are presumed to depend on η_1.

By way of a simple experiment, a pinhole microphone assembly was flush mounted in the wall of a subsonic wind tunnel. The tunnel speed was adjusted so that the probe was in the transition zone of the wall boundary layer. An intermittency detector enabled us to generate, electronically, the indicator function and to determine γ and N. A real-time correlation analyzer was used to compute the auto-correlation function of $I(x_1,t)$. The result of this experiment is shown in Fig. 6 along with the prediction given by Eq. (31) for $\xi_1 = 0$. The agreement is seen to be quite good.

With regard to the γ and N distributions, we note that Emmons [9] first discussed them and developed a probabilistic model to predict them. He assumed the existence of a source-rate density function, $g(x_0,z_0,t)$, which specifies the rate of production of turbulent point-source bursts per unit area on the surface at position $x_1 = x_0$, $x_3 = z_0$, and time t_0. In his example, Emmons assumed $g(x_0,z_0,t_0)$ to be constant; however, a later investigation by Narasimha [30] which made use of the data of Ref. [10], showed that $g(x_0,z_0,t_0)$ is more accurately described by a Delta function. In particular, $g(x_1) = n\delta(x_1-x_0)$, where n is defined as the number of sources per unit length per unit time along the line $x_1 = x_0$. Farabee, et.al [11] made use of this form of g in deriving emperical relations for γ and N. They are:

$$\gamma(Z) = 1-e^{-4.185Z^2} \tag{32}$$

and

$$N(Z) = 1.272 \frac{u_0}{\Delta x} Ze^{-4.185Z^2} , \tag{33}$$

where $Z = \eta_1/\Delta x$. Figure 7 shows plots of N and γ as computed from Eq's. (32) and (33).

The flare parameter, α^*, in Eq. (31) is considerably more difficult to predict because of the lack of experimental data. Under a fully-developed turbulent boundary layer, we can estimate α^* from Fig. 7 of Blake's [29] wall pressure data. The smooth-wall decay envelope can be approximated by $\exp(-\xi_1/2\delta^*)$, where δ^* is the displacement thickness. Thus, we let α^* $(Z \gtrsim 1) = (2\delta^*)^{-1}$. Within the transition zone, we can make use of the space-time correlations measured by Shivitz, ibid, Fig. 24. Here, $Z = 0.6$ and the decay envelope can be approximated by $\exp(-\xi_1/110\delta^*)$, where the δ^* is that measured shortly downstream of where the flow became fully turbulent; hence, α^* $(Z = 0.6) = (110\delta^*)^{-1}$. Farther upstream in the transition zone, we can only speculate as to what value α^* may have. Because there will be fewer bursts of turbulence as $Z \to 0$, we might anticipate that the moving-axis decorrelation becomes less severe, meaning α^* should decrease as $Z \to 0$. We will assume this to be the case, and also, that α^* can never become smaller than $(\Delta x)^{-1}$; thus, we let α^* $(Z = 0) = (\Delta x)^{-1}$. Using the three values of α^* discussed above, and the values of δ^* and Δx measured by Shivitz, the following equation for α^* can be constructed:

$$\alpha^* = (1+83.35Z^8)/\Delta x \quad , \tag{34}$$

which is shown graphically in Fig. 8.

The space-time correlation function given by Eq. (31) was computed for $Z = 0.6$ and $u_0/\Delta x = 467$ Hz (typical value for water). Figure 9 shows the resulting three-dimensional surface.

2. Integration of Eq. (29)

If we now substitute Eq. (31) into Eq. (29), and change the variable $(\tau-\xi_1/u_c)$ to τ', we then have:

$$\frac{\partial G(r,f)}{\partial x_3} \simeq \frac{\omega^2\cos^2\theta\sigma^2}{4\pi^2 r^2 c^2} \int_0^{\Delta x} \eta_1\gamma \int_{-\eta_1}^{\Delta x-\eta_1} e^{-\alpha^*|\xi_1|} e^{ik_c\xi_1} \int_{-\infty}^{\infty} e^{-2N|\tau'|} e^{i\omega\tau'}\, d\tau'\, d\xi_1\, d\eta_1$$

where $k_c = \omega/u_c$. The last integral is well-known and equal to $2N/(4N^2+\omega^2)$. Because the power spectrum must be real, the above equation reduces to:

$$\frac{\partial G(r,f)}{\partial x_3} \simeq \frac{\omega^2\cos^2\theta\sigma^2}{2\pi^2 r^2 c^2} \int_0^{\Delta x} \frac{\eta_1\ \gamma\ N}{4N^2+\omega^2} \left\{ \int_{-\eta_1}^{0} e^{\alpha^*\xi_1}\cos k_c\xi_1 d\xi_1 + \int_0^{\Delta x-\eta_1} e^{-\alpha^*\xi_1}\cos k_c\xi_1 d\xi_1 \right\} d\eta_1 . \quad (35)$$

The integrations over ξ_1 can be performed. Without showing the details, but noting that the following identity was used:

$$a\sin\theta + b\cos\theta = \sqrt{a^2+b^2}\,\sin(\theta+\tan^{-1}\frac{b}{a}) \quad ,$$

and that the change of variable from η_1 to $Z = \eta_1/\Delta x$ was also made, Eq. (35) becomes:

$$\frac{\partial G(r,f)}{\partial x_3} \simeq \frac{\sigma^2(x_0)\cos^2\theta u_0(\Delta x)^2}{2\pi^2 r^2 c^2} F(k_c\Delta x, \alpha^*\Delta x, u_c/u_0) \quad , \quad (36)$$

with

$$F(k_c\Delta x,\alpha^*\Delta x,u_c/u_0) = (k_c\Delta x)^2 \int_0^1 \frac{1.272Z^2(1-e^{-4.185Z^2})e^{-4.185Z^2}}{\left[6.472\left(\frac{u_0}{u_c}\right)^2 Z^2 e^{-8.37Z^2}+(k_c\Delta x)^2\right]\sqrt{(\alpha^*\Delta x)^2+(k_c\Delta x)^2}}$$

$$\cdot\left\{\frac{2\alpha^*\Delta x}{\sqrt{(\alpha^*\Delta x)^2+(k_c\Delta x)^2}} - e^{-\alpha^*\Delta xZ}\sin(k_c\Delta xZ-\phi) + e^{-\alpha^*\Delta x(1-Z)}\sin[k_c\Delta x(1-Z)-\phi]\right\} dZ \ , \quad (37)$$

and $\phi = \tan^{-1}(\alpha^*\Delta x/k_c\Delta x)$. In the development of Eq. (36), it has been assumed that u_c/u_0 is independent of frequency.

Equation (37) cannot be integrated conveniently; however, because of its non-dimensional form, it need only be integrated once for a few discrete values of u_c/u_0 and a range of $k_c\Delta x$ [assuming Eq. (34) describes the behavior of $\alpha^*\Delta x$]. This integration has been performed for $u_c/u_0 = 0.6$ and 0.8 by Simpson's rule. The result is presented graphically in Fig. 10. We see that boundary-layer transition generates significant noise only in a frequency band centered about $f_o = u_c/2\pi\Delta x$.

Because $\sigma(x_0)$ is proportional to ρu_0^2, Eq. (36) suggests that the spectral level increases according to u_0^5 for constant Δx. However, Eq. (27) suggests that Δx is inversely proportional to u_0, so Eq. (36) predicts a u_0^3 velocity dependence even though the source of noise is dipole. The reason for this unexpected behavior is that the solution is derived in terms of the detailed hydrodynamics. These details result in a source area that changes with velocity. Thus, to be consistent with less-rigorous, flow noise order of magnitude estimates, the radiation-field pressure should be normalized by the area of the source region, which is proportional to Δx. The mean-square value of the sound pressure radiated per unit area would then be given by the integration of Eq. (36) over frequency divided by $(\Delta x)^2$. A 5th power velocity dependence would thus be retained.

E. Radiation Efficiency

The radiation efficiency, $\eta_{tr.}$, is defined as the ratio of acoustic power, N_a, radiated to the farfield-to-the work expended per unit time by the hydrodynamic motions within the acoustic source region, N_h. By re-writing Eq. (36) in the form:

$$\frac{\partial G(r,f)}{\partial x_3} = \cos^2\theta \, \langle p_0^2 \rangle \quad ,$$

we see that

$$N_a = \int_0^\infty \frac{\langle p_0^2 \rangle}{\rho c} \, d\omega \int_0^{2\pi} \int_0^{\pi} \cos^2\theta r^2 \sin\theta d\theta d\phi \quad . \tag{38}$$

Upon substituting for $\langle p_0^2 \rangle$, Eq. (38) reduces to:

$$N_a \simeq \frac{2\sigma^2 u_0^2 \Delta x}{3\pi\rho c^3} \overline{F} \quad , \tag{39}$$

where

$$\overline{F} = \int_0^\infty F(k_c\Delta x, \alpha^*\Delta x, u_c/u_0) \, d(k_c\Delta x) \quad .$$

The magnitude of $\overline{F}$ is denoted in Fig. 10 for each of the two convection speed ratios considered. Essentially, $\overline{F}$ is independent of u_c/u_0 and is of order 0.1.

Because Eq. (39) is the acoustic power radiated per unit spanwise width of transitional flow, it is necessary to compute the hydrodynamic power also on a per unit width basis. The energy expended per unit time per unit width by transitional flow may be expressed by:

$$N_h = u_0 \int_{x_0}^{x_0+\Delta x} \tau_0 \, dx_1 \tag{40}$$

where τ_0 is the mean value of the wall shear stress. Because bursting flow occurs between the limits of integration, we would expect that

$$\tau_o (x_1) = \tau_T (x_1)\gamma(x_1) + [1-\gamma(x_1)] \tau_L (x_1) \quad . \tag{41}$$

Because

$$\tau_o = (\tau_T - \tau_L) \gamma + \tau_L \quad ,$$

where $(\tau_T - \tau_L) = \sigma \simeq 0.9\tau_T$, we let

$$\tau_o (x_1) \simeq \gamma(x_1) \sigma (x_1) \quad . \tag{42}$$

The intermittency distribution can be calculated using Eq. (32). Again we use Eq. (28) to arrive at

$$N_h = u_0 \Delta x \sigma(x_0) \left[1 - \int_0^1 e^{-4.185Z^2} dZ \right] \quad .$$

Through a change of integration variable, the above integral can be expressed in terms of the error function, i.e.,

$$N_h \simeq u_0 \Delta x \sigma [1-0.488 \frac{\sqrt{\pi}}{2} \text{erf}(2.048)]$$

$$\simeq 0.572\, u_0 \Delta x\, \sigma \quad . \tag{43}$$

The radiation efficiency is now obtained by dividing Eq. (39) by Eq. (43), which results in

$$\eta_{tr.} \simeq 0.37 \frac{\sigma u_0 \overline{F}}{\rho c^3} \quad . \tag{44}$$

Again noting that $\sigma \sim \rho u_0^2$, we see that the radiation efficiency is proportional to the cube of the free-stream Mach number. This is analogous to what Landahl [7] found for the shear stress contribution to fully-developed turbulent boundary-layer radiated noise, i.e.,

$$\eta_{TBL} \sim \frac{u^*}{u_0} M_*^3 \quad , \tag{45}$$

where u_* is the friction velocity and $M_* = u_*/c$.

We would like to compare the radiation efficiency of transitional flow to that of a fully-developed turbulent boundary layer (TBL) flow. Equation (45) cannot be used in this comparison due to the lack of a proportionality factor. An analysis given by Tam [31], however, may be used in this regard. Tam did not derive an explicit expression for the efficiency, but did give an expression for the acoustic power generated per unit surface area of boundary layer turbulence. In particular,

$$N_{TBL} = \frac{4\pi\tau_T^2}{\rho c} \int_0^\infty F(S,M)\, dS \quad , \tag{46}$$

where the integral is presented graphically in Reference [31] as a function of Mach number, M. Tam concluded that the magnitude of this integral increases rather rapidly with Mach number (slightly faster than M^2). We have thus been able to approximate it by:

$$\int_0^\infty F(S,M)\, dS \simeq 0.015M^2 \quad (M > 0) \quad . \tag{47}$$

The hydrodynamic power generated per unit surface area of boundary layer turbulence is given by $u_0\tau_T$, so we would expect that:

$$\eta_{TBL} \simeq \frac{0.188\ \tau_T\ M^2}{\rho c u_0} \quad . \tag{48}$$

By letting $\sigma \simeq \tau_T$, we find that

$$\eta_{tr.} \simeq 1.97\ \overline{F}\ \eta_{TBL} \simeq 0.2\ \eta_{TBL} \quad . \tag{49}$$

This result implies that the wall shear stress fluctuations that occur in intermittent transition zone flow generate noise less efficiently than do the supersonic Fourier components of the normal stress fluctuations [31] in a fully-developed turbulent boundary layer.

III. EXAMPLE

In order to verify the analysis presented in this paper, one must conduct a very sophisticated experiment. This author envisions such an experiment as being composed of a large, nearly rigid, thin flat plate mounted in an anechoic wind tunnel (air is better than water because of the rigidity requirement). The span of the plate must be very large as to minimize the edge noise received, say at the center of the plate. Because the theory predicts a cosine directivity curve, one must use flush mounted microphones in order to receive the peak sound level. They should be placed in the laminar flow regime of the plate's boundary layer as to minimize near-field pressure fluctuation effects. Perhaps most importantly, the operating Reynolds number should be adjusted so that fully-developed turbulent flow occurs very near the trailing edge of the plate ($x_1 + \Delta x$ = length of plate). The trailing edge must be designed to minimize, as much as possible, any unsteady wake flow. Unfortunately, an experiment such as this one has not yet been carried out.

Nevertheless, it is tempting at this point, to make a prediction using the subject theory for a situation in which noise was measured flush to the surface and within the laminar boundary layer of a test vehicle. We choose those data presented by Nisewanger and Sperling [32]. In their experiment, a buoyantly-propelled axisymmetric body was instrumented with flush-mounted hydrophones and noise spectra at various locations on the surface were measured in fresh water at a vehicle speed of 19.4 m/s. The transition point was found to be at an arc length distance of 16 cm. Equation (27) is used to calculate Δx; we find it to be 5.8 cm using the kinematic viscosity for fresh water at 21°C. Measurement station no. 4 of Ref. 32 is selected because it is in the laminar flow region, 2.6 cm forward of the transition point. Letting $\theta = 0°$, $u_c/u_0 = 0.8$, and multiplying Eq. (36) by the circumference of the test body, the resulting comparison of theory and experiment is shown in Fig. 11.

As might be expected, the agreement is not very good. The differences in level may be attributable to several reasons. Because the test vehicle supports a substantial area of fully-developed turbulent boundary layer flow, the data may be contaminated by this source of noise. Also, as noted by Nisewanger and Sperling, approximately 50 percent of the measured flow noise is due to shell vibrations. From the more fundamental point of view, the shear stress mechanism of sound generation by a transition zone may not be the only mechanism involved. We neglected the Reynolds stress contributions through an argument of relative efficiency between dipole and quadrupole sources. It would seem reasonable that the fluctuating shear stress, being a viscous quantity, may be considerably smaller than the fluctuating Reynolds stress; perhaps even small enough, that the relative difference in radiation efficiency is out-weighed.

IV. CONCLUSIONS

We have presented an analysis of the radiated sound due to boundary-layer transition. Our principle assumptions were that the surface is infinite in extent, planar, and rigid, that the transition process includes a finite region intermittent flow where the boundary layer fluctuates randomly between laminar and turbulent, and that it is this intermittent flow that generates the noise. Through use of Lighthill's analogy, we showed that the fluctuations between laminar and turbulent boundary-layer flow give rise to dipole, quardupole, and octupole noise sources. On the basis of a very low Mach number assumption, we treated only the dipole contribution in detail; this contribution being due to the fluctuating wall shear stresses. We assumed that the flow is statistically homogeneous in the spanwise directions, non-homogeneous in the streamwise direction, and stationary, but Poisson distributed in time. The power spectral density for the acoustic pressure radiated per unit

spanwise width was derived. The level of the mean-square radiated pressure was found to depend upon the square of the difference between the turbulent wall shear stress and the laminar wall shear stress that would occur at the beginning of transition, upon the square of the streamwise distance over which turbulent bursts occur, and upon the free-stream velocity. The spectrum rises at 6 dB/octave at low frequencies and drops off at 6 dB/octave at high frequencies. A broad peak is centered about $k_c \Delta x = 1.0$. An expression for the radiation efficiency was derived and compared to the radiation efficiency of a fully-developed turbulent boundary layer. This comparison showed that transition generates noise at approximately 20 percent the efficiency of fully-developed turbulent boundary layer flow.

We compared a prediction using this theory with the noise spectrum measured near the laminar-to-turbulent transition region of a buoyantly-propelled flow noise research vehicle. The agreement was considered to be poor. Based on this comparison and on the magnitude of the radiation efficiency it can be concluded that the shear stress fluctuations that occur in natural boundary-layer transition are not strong sound radiators. However, boundary-layer transition is a very complicated hydrodynamic phenomenon, and the neglect of fluctuating Reynolds stresses on the supposition that they give rise to inefficient quardupoles and octupoles may not be fully justified. A detailed examination of the first term of Eq. (9) appears to be required but the modeling of $u_i u_j$ in an intermittent flow regime may prove to be very difficult. In order to simplify this task, it may prove expedient to first investigate the third and sixth terms of Eq. (10) which describe the normal stress contributions. Such analysis must be performed in wavenumber/frequency space so that those Fourier components with phase velocities (ω/k) greater than or equal to the velocity of sound can be identified (if present). It would be these components that lead to sound radiation; any others would cause near-field pressure fluctuations.

In any event, additional experimentation is required in order to support or disprove the notion that boundary-layer transition is an important source of low Mach number flow noise. The space-time correlation functions at various locations within a transition zone should be measured. These functions would not only aid in the modeling presented in this paper, but would provide the groundwork necessary to proceed with further analysis such as that suggested above.

REFERENCES

1. J. E. Ffowcs Williams, "Flow Noise," in Underwater Acoustics, Vol. 2, edited by V. M. Albers, (Plenum Press, New York, 1967) Chapter 6, pp. 89-102.

2. G. P. Haddle and E. J. Skudrzyk, "The Physics of Flow Noise," J. Acoust. Soc. Am., 46, 130-157 (1969).

3. G. C. Lauchle, "Noise Generated by Axisymmetric Turbulent Boundary-Layer Flow," J. Acoust. Soc, Am., 61, 694-702 (1977).

4. I. I. Dolgova," Sound Field Radiated by a Tollmien - Schlichting Wave," Sov. Phys. Acoust., 23, 259-260 (1977).

5. T. Brooke Benjamin, "The Development of Three-Dimensional Disturbances in an Unstable Film of Liquid Flowing Down an Inclined Plane," J. Fluid Mech., 10, 401-419 (1961).

6. M. J. Lighthill, "On Sound Generated Aerodynamically, II: Turbulence as a Source of Sound," Proc. Roy. Soc. Lond. A222, 1-32 (1954).

7. M. T. Landahl, "Wave Mechanics of Boundary Layer Turbulence and Noise," J. Acoust. Soc. Am., 57, 824-831 (1975).

8. D. Ross, Mechanics of Underwater Noise, (Pergamon Press, New York, 1976), p. 51.

9. H. W. Emmons, "The Laminar-Turbulent Transition in a Boundary Layer - Part I," J. Aero. Sci., 18, 490-498 (1951).

10. G. B. Schubauer and P. S. Klebanoff, "Contributions on the Mechanics of Boundary Layer Transition," NACA Report 1289, 1956.

11. T. M. Farabee, M. J. Casarella and F. C. DeMetz, "Source Distribution of Turbulent Bursts During Natural Transition," David W. Taylor Naval Ship Research and Development Center Report SAD-89E-1942, August 1974.

12. H. Schlichting, Boundary-Layer Theory (McGraw-Hill Book Co., New York, 1968), 6th ed., pp. 698, 128.

13. N. Curle, "The Influence of Solid Boundaries Upon Aerodynamic Sound," Proc. Roy. Soc. Lond. A231, 505-514 (1955).

14. A. Powell, "Aerodynamic Noise and the Plane Boundary," J. Acoust. Soc. Am., 32, 982-990 (1960).

15. J. Laufer, J. E. Ffowcs Williams and S. Childress, "Mechanism of Noise Generation in the Turbulent Boundary Layers," AGARD ograph 90 (1964).

16. L. S. G. Kovasznay, V. Kibens and R. F. Blackwelder, "Large-Scale Motion in the Intermittent Region of a Turbulent Boundary Layer," J. Fluid Mech., 41, 283-325 (1970).

17. P. A. Libby, "On the Prediction of Intermittent Turbulent Flows," J. Fluid Mech., 68, 273-295 (1975).

18. R. E. Lessman, "Intermittent Transition Flow in a Boundary Layer," AIAA J., 15, 1656-1658 (1977).

19. Kovasznay, et.al, ibid., p. 308, investigated the space-time correlation functions for $I(x_2,t)$ that occur through the outer shear flow area of fully-developed turbulent flow. These results are not directly applicable to the present analysis.

20. K. K. Chen and N. A. Thyson, "Extension of Emmons' Spot Theory to Flows on Blunt Bodies," AIAA J., 9, 821-825 (1971).

21. W. Schottky, "Theory of Shot Effect," Ann. Phys., 57, 541-568 (1918).

22. S. Dhawan and R. Narasimha, "Some Properties of Boundary Layer Flow During the Transition from Laminar to Turbulent Motion," J. Fluid Mech., 3, 418-436 (1958).

23. J. S. Bendat and A. G. Piersol, Random Data: Analysis and Measurement Procedures, (John Wiley & Soms, Inc., New York, 1971) p. 23.

24. G. M. Corcos, "Resolution of Pressure in Turbulence," J. Acoust. Soc. Am., 35, 192-199 (1963).

25. D. G. Crighton, "Basic Principles of Aerodynamic Noise Generation," Prog. Aerosp. Sci. 16, 31-96 (1975).

26. W. F. Shivitz, "An Experimental Investigation of Artificially - Induced Transition to Turbulence on a Body of Revolution," Master of Science Thesis in Aerospace Engineering, The Pennsylvania State University, (1975).

27. F. C. DeMetz and M. J. Casarella, "An Experimental Study of the Intermittent Properties of the Boundary Layer Pressure Field During Transition on a Flat Plate," David W. Taylor Naval Ship Research and Development Center Report 4140, AD-775-299, November 1973.

28. S. O. Rice, "Mathematical Analysis of Random Noise," Bell Sys. Tech. J. 23, 282-332 (1944).

29. W. K. Blake, "Turbulent Boundary-Layer Wall-Pressure Fluctuations on Smooth and Rough Walls," J. Fluid Mech. 44, 637-660 (1970).

30. R. Narasimha, "On the Distribution of Intermittency in the Transition Region of a Boundary Layer," J. Aero. Sci. 24, 711-712 (1957).

31. C. K. W. Tam, "Intensity, Spectrum and Directivity of Turbulent Boundary Layer Noise," J. Acoust. Soc. Am. 57, 24-34 (1975).

32. C. R. Nisewanger and F. B. Sperling, "Flow Noise Inside Boundary Layers of Buoyancy-Propelled Test Vehicles," NAVWEPS Report 8519, NOTS TP 3511 (1965).

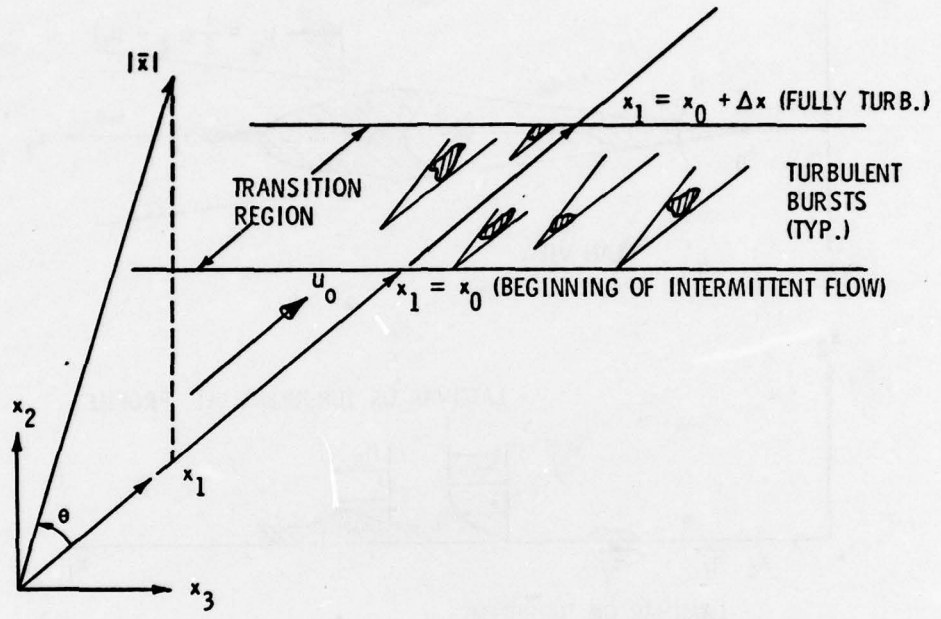

Figure 1. Definition of the coordinates used and a schematic representation of the transition process.

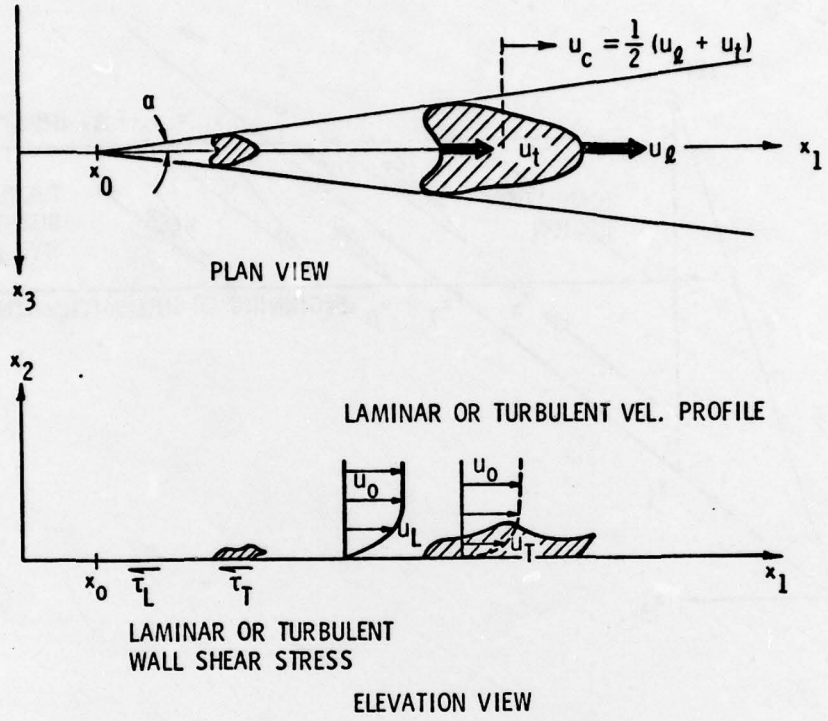

Figure 2. Schematic description of turbulent bursts and the boundary layer development.

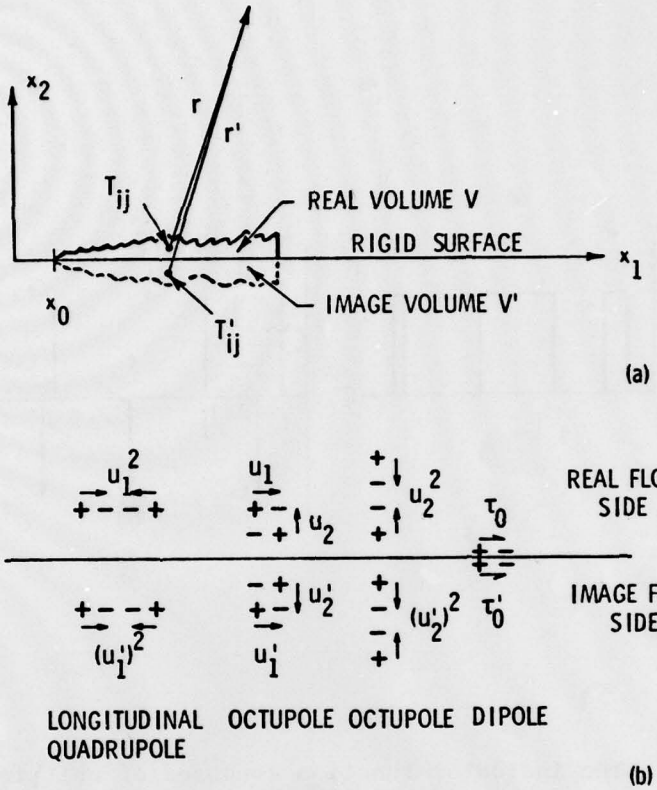

Figure 3. (a) A schematic representation of the image flow concept; and,

(b) the way in which multipole sources in the real flow combine with equivalent sources in the image flow.

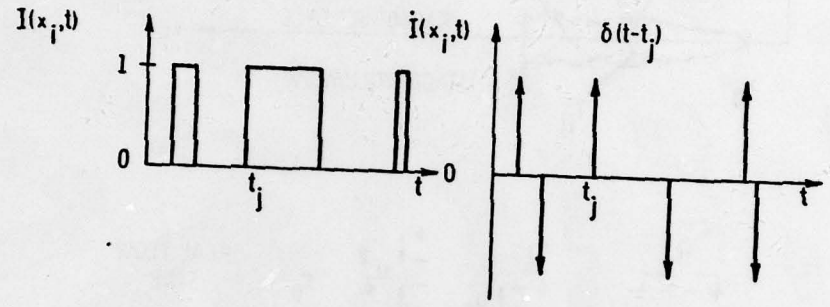

Figure 4. The indicator function composed of unit impulse functions and its first time derivative.

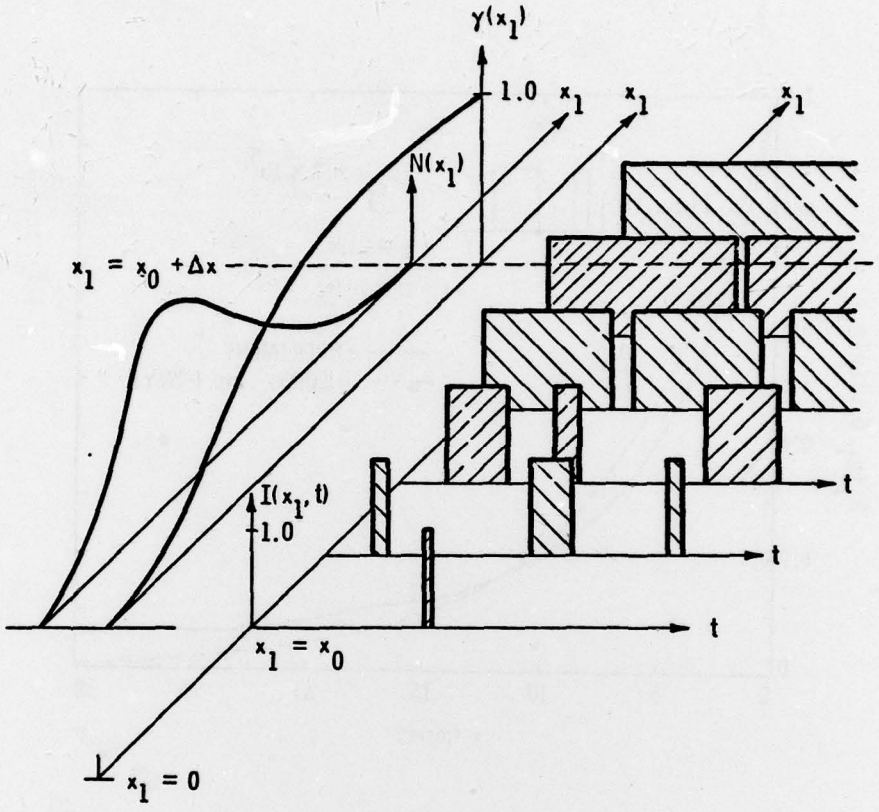

Figure 5. A schematic representation of $I(x_1,t)$ in space and time, where γ is its time average value and N is the expected number of bursts per unit time.

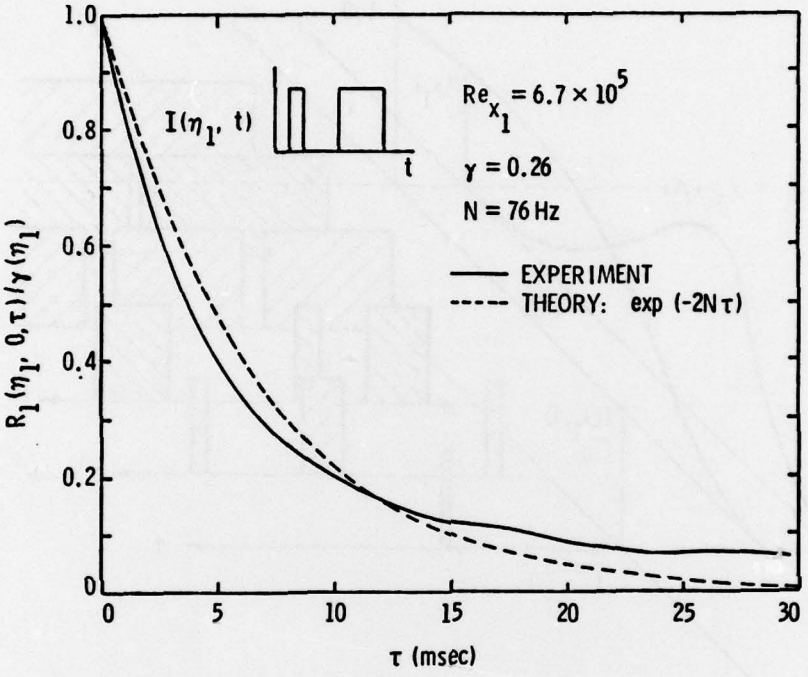

Figure 6. The autocorrelation function of $I(x_1,t)$ as measured in a transitional flow and as computed for a Poisson process.

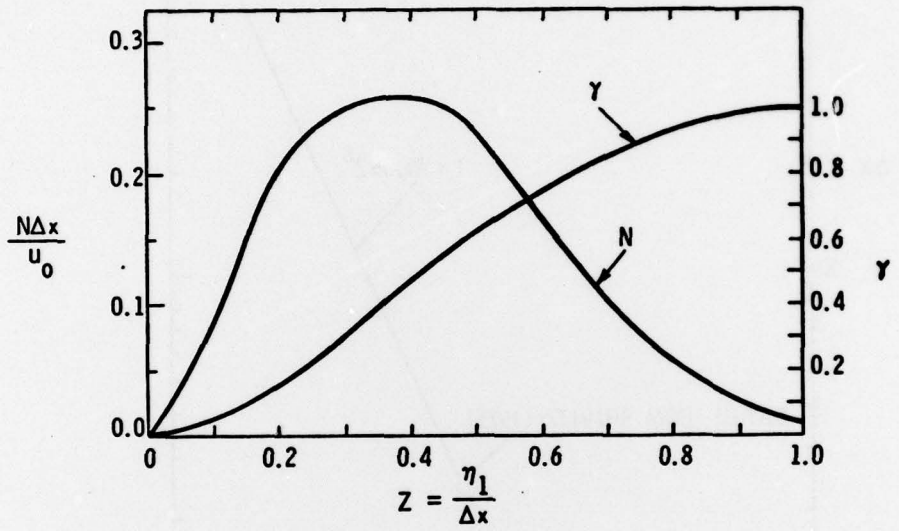

Figure 7. The intermittency and burst frequency distributions from Equations (32) and (33).

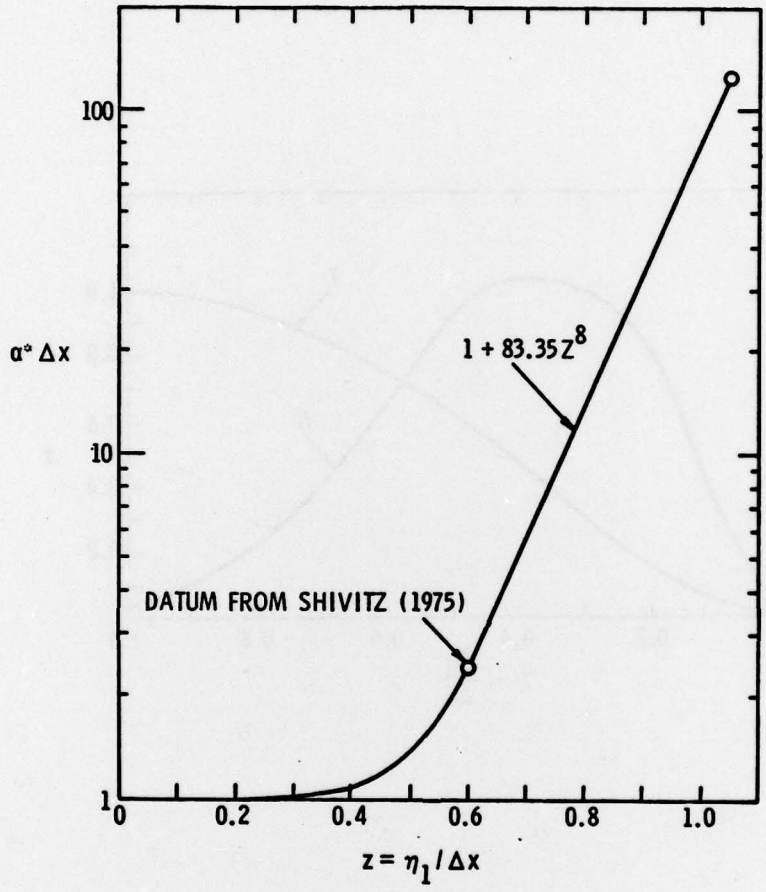

Figure 8. Normalized flare parameter $\alpha^* \Delta x$ as a function of the normalized position in the transitional region.

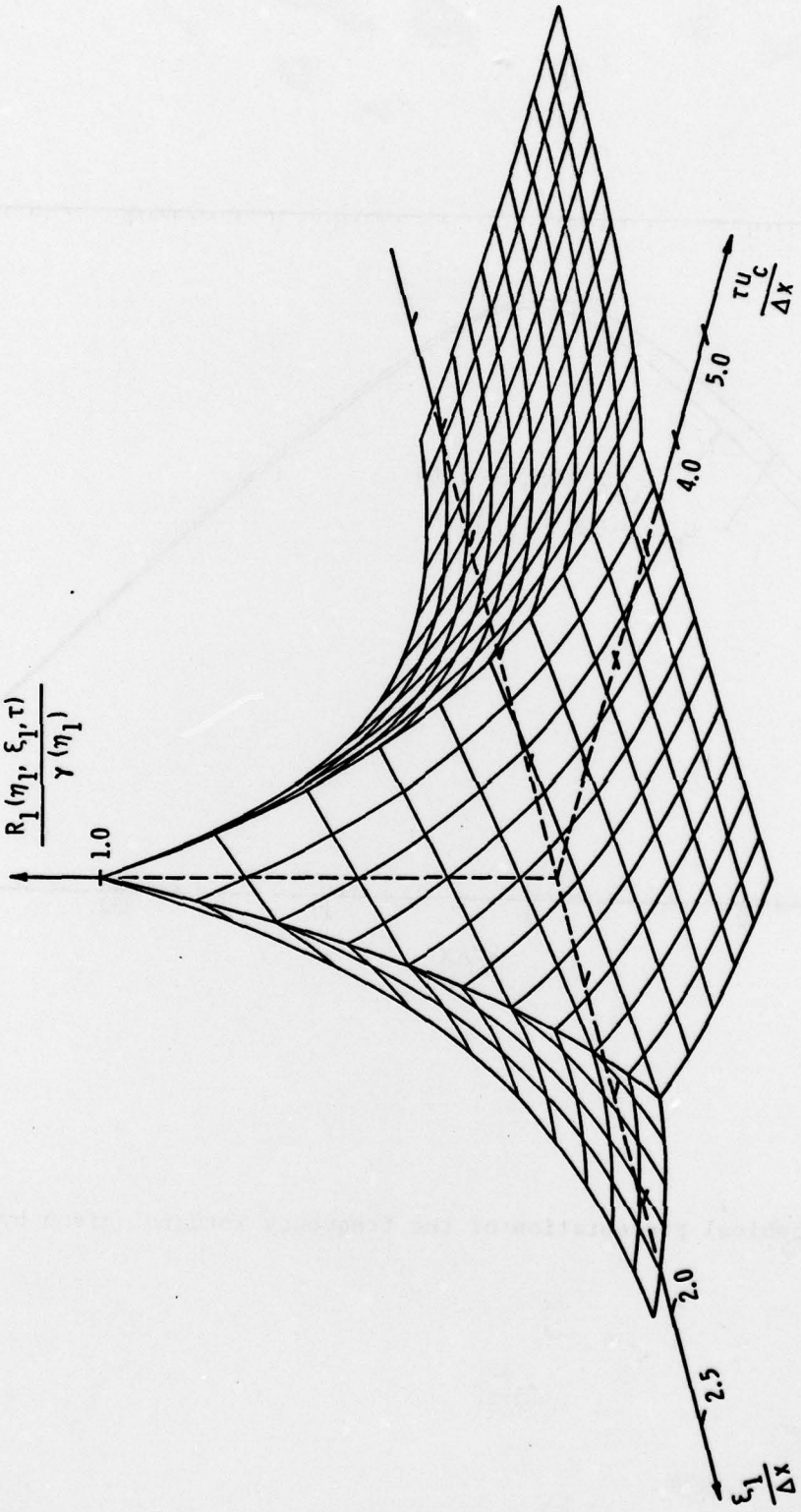

Figure 9. Graphical presentation of the longitudinal space-time correlation function used in the noise analysis [from Eq. (31)].

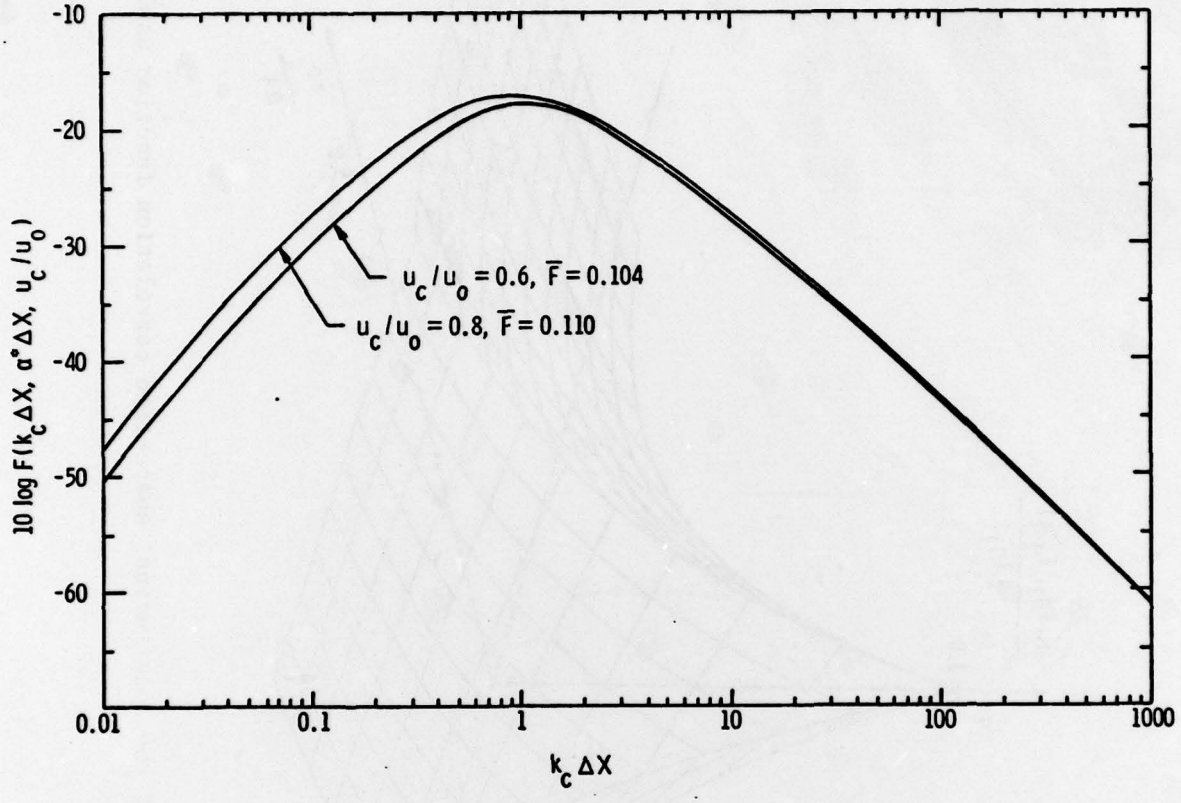

Figure 10. Graphical presentation of the frequency integral given by Eq. (37).

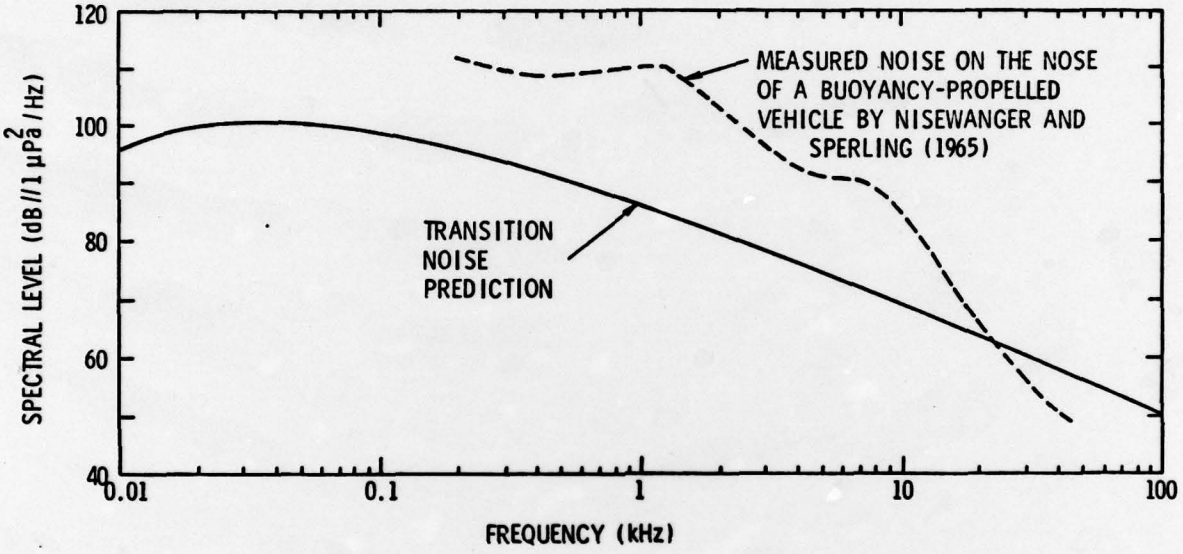

Figure 11. Comparison of the theory with experimental spectra measured on the surface of a buoyantly-propelled flow noise research vehicle [32].

DISTRIBUTION LIST FOR UNCLASSIFIED TM 79-135 by G. C. Lauchle, dated 23 July 1979.

Commander
Naval Sea Systems Command
Department of the Navy
Washington, DC 20362
Attn: Library
Code NSEA-09G32
(Copies No. 1 and 2)

Naval Sea Systems Command
Attn: C. G. McGuigan
Code NSEA-63R-27
(Copy No. 3)

Naval Sea Systems Command
Attn: L. N. Benen
Code NSEA-524
(Copy No. 4)

Naval Sea Systems Command
Attn: E. J. McKinney
Code NSEA-0342
(Copy No. 5)

Naval Sea Systems Command
Attn: E. G. Liszka
Code NSEA-63R1
(Copy No. 6)

Naval Sea Systems Command
Attn: G. Sorkin
Code NSEA-63R
(Copy No. 7)

Naval Sea Systems Command
Attn: T. E. Peirce
Code NSEA-63R-31
(Copy No. 8)

Naval Sea Systems Command
Attn: J. G. Juergens
Code NSEA-05H
(Copy No. 9)

Naval Sea Systems Command
Attn: H. C. Claybourne
Code NSEA-05H
(Copy No. 10)

Naval Sea Systems Command
Attn: A. R. Paladino
Code NSEA-05H
(Copy No. 11)

Naval Sea Systems Command
Attn: D. L. Creed
Code NSEA-03132A
(Copy No. 12)

Commander
Naval Ship Engineering Center
Department of the Navy
Washington, DC 20360
Attn: W. L. Louis
Code NSEC-6136B
(Copy No. 13)

Naval Ship Engineering Center
Attn: F. J. Welling
Code NSEC-6144
(Copy No. 14)

Commanding Officer
Naval Underwater Systems Center
Newport, RI 02840
Attn: C. N. Pryor
Code 01
(Copy No. 15)

Naval Underwater Systems Center
Attn: D. Goodrich
Code 36315
(Copy No. 16)

Naval Underwater Systems Center
Attn: R. J. Kittredge
Code 36313
(Copy No. 17)

Naval Underwater Systems Center
Attn: J. Miguel
Code 36315
(Copy No. 18)

Naval Underwater Systems Center
Attn: B. J. Myers
Code 36311
(Copy No. 19)

Naval Underwater Systems Center
Attn: R. H. Nadolink
Code 36315
(Copy No. 20)

Naval Underwater Systems Center
Attn: D. A. Quadrini
Code 36314
(Copy No. 21)

DISTRIBUTION LIST FOR UNCLASSIFIED TM 79-135 by G. C. Lauchle, dated 23 July 1979.

Naval Underwater Systems Center
Attn: E. J. Sullivan
Code 36311
(Copy No. 22)

Naval Underwater Systems Center
Attn: R. Trainor
Code 36314
(Copy No. 23)

Naval Underwater Systems Center
Attn: F. White
Code 36301
(Copy No. 24)

Naval Underwater Systems Center
Attn: Library
Code 54
(Copy No. 25)

Commanding Officer
Naval Ocean Systems Center
San Diego, CA 92152
Attn: J. W. Hoyt
Code 2501
(Copy No. 26)

Naval Ocean Systems Center
Attn: M. M. Reischman
Code 2542
(Copy No. 27)

Naval Ocean Systems Center
Attn: G. L. Donohue
Code 2542
(Copy No. 28)

Commander
David W. Taylor Naval Ship R&D Center
Department of the Navy
Bethesda, MD 20084
Attn: Code 1505
(Copy No. 29)

David W. Taylor Naval Ship R&D Center
Attn: W. B. Morgan
Code 154
(Copy No. 30)

David W. Taylor Naval Ship R&D Center
Attn: R. A. Cumming
Code 1544
(Copy No. 31)

David W. Taylor Naval Ship R&D Center
Attn: J. H. McCarthy
Code 1552
(Copy No. 32)

David W. Taylor Naval Ship R&D Center
Attn: T. E. Brockett
Code 1544
(Copy No. 33)

David W. Taylor Naval Ship R&D Center
Attn: Y. T. Shen
Code 1524
(Copy No. 34)

David W. Taylor Naval Ship R&D Center
Attn: M. M. Sevik
Code 19
(Copy No. 35)

David W. Taylor Naval Ship R&D Center
Attn: W. K. Blake
Code 1942
(Copy No. 36)

David W. Taylor Naval Ship R&D Center
Attn: T. M. Farabee
Code 1942
(Copy No. 37)

David W. Taylor Naval Ship R&D Center
Attn: F. C. DeMetz
Code 1942
(Copy No. 38)

David W. Taylor Naval Ship R&D Center
Attn: M. J. Casarella
Code 1942
(Copy No. 39)

Officer-In-Charge
David W. Taylor Naval Ship R&D Center
Department of the Navy
Annapolis Laboratory
Annapolis, MD 21402
Attn: J. G. Stricker
Code 2721
(Copy No. 40)

Commander
Naval Surface Weapon Center
Silver Spring, MD 20910
Attn: G. C. Gaunaurd
Code R-31
(Copy No. 41)

DISTRIBUTION LIST FOR UNCLASSIFIED TM 79-135 by G. C. Lauchle, dated 23 July 1979.

Naval Surface Weapon Center
Attn: Library
(Copy No. 42)

Office of Naval Research
Department of the Navy
800 N. Quincy Street
Arlington, VA 22217
Attn: H. Fitzpatrick
Code 438
(Copy No. 43)

Office of Naval Research
Attn: R. D. Cooper
Code 438
(Copy No. 44)

Naval Research Laboratory
Washington, DC 20390
Attn: R. J. Hansen
Code 20375
(Copy No. 45)

Defense Documentation Center
5010 Duke Street
Cameron Station
Alexandria, VA 22314
(Copies No. 46 - 57)

National Bureau of Standards
Aerodyanmics Section
Washington, DC 20234
Attn: P. S. Klebanoff
(Copy No. 58)

Rand Corporation
1700 Main Street
Santa Monica, CA 90406
Attn: C. Gazley
(Copy No. 59)

Jet Propulsion Laboratory
4800 Oak Grove Drive
Pasadena, CA 91108
Attn: L. M. Mack
(Copy No. 60)

Hersh Acoustical Engineering
9545 Cozycroft Avenue
Chatsworth, CA 91311
Attn: A. Hersh
(Copy No. 61)

Dynamics Technology, Inc.
3838 Carson Street, Suite 110
Torrance, CA 90503
Attn: W. N. Haigh
(Copy No. 62)

Dynamics Technology, Inc.
Attn: D. R. S. Ko
(Copy No. 63)

Bolt Beranek and Newman
50 Moulton Street
Cambridge, MA 20136
Attn: N. Brown
(Copy No. 64)

Bolt Beranek and Newman
Attn: D. Chase
(Copy No. 65)

Bolt Beranek and Newman
Attn: K. L. Chandiramani
(Copy No. 66)

Kentex International, Inc.
2054 University Avenue - #301
Berkeley, CA 94704
Attn: S. Yang
(Copy No. 67)

Bell Laboratories
Whippany Road
Whippany, NJ 07981
Attn: J. G. Berryman
(Copy No. 68)

Massachusetts Institute of Technology
77 Massachusetts Avenue
Cambridge, MA 02139
Attn: Prof. Patrick Leehey
Department of Ocean Engineering
Room 5-222
(Copy No. 69)

Cornell University
Sibley School of Mechanical and
Aeronautical Engineering
Upson Hall
Ithaca, NY 14850
Attn: Dr. J. L. Lumley
(Copy No. 70)

DISTRIBUTION LIST FOR UNCLASSIFIED TM 79-135 by G. C. Lauchle, dated 23 July 1979

University of Minnesota
St. Anthony Falls Hydraulic Laboratory
Mississippi River at 3rd Ave. S.E.
Minneapolis, MN 55414
Attn: R. E. A. Arndt
(Copy No. 71)

University of Minnesota
Attn: Lorenz G. Straub Memorial Library
(Copy No. 72)

University of Leeds
Department of Applied Mathematical Studies
Leeds LS29JT, England
Attn: Dr. D. G. Crighton
(Copy No. 73)

A. G. Fabula
5497 Coral Reef Avenue
La Jolla, CA 92037
(Copy No. 74)

Applied Research Laboratory
The Pennsylvania State University
Post Office Box 30
State College, PA 16801
Attn: B. R. Parkin
(Copy No. 75)

Applied Research Laboratory
Attn: E. J. Skudrzyk
(Copy No. 76)

Applied Research Laboratory
Attn: G. H. Hoffman
(Copy No. 77)

Applied Research Laboratory
Attn: F. H. Fenlon
(Copy No. 78)

Applied Research Laboratory
Attn: G. C. Lauchle
(Copy No. 79)

Applied Research Laboratory
Garfield Thomas Water Tunnel File
(Copy No. 80)